

# Relayed Hyperpolarization for Zero-Field Nuclear Magnetic Resonance

## Authors

Erik T. Van Dyke,<sup>1,2</sup> James Eills,<sup>1,2,3</sup> Román Picazo-Frutos,<sup>1,2</sup> Kirill F. Sheberstov,<sup>1,2</sup>  
Yinan Hu,<sup>1,2</sup> Dmitry Budker,<sup>1,2,4</sup> and Danila A. Barskiy<sup>1,2,\*</sup>

## Affiliations

1. Institut für Physik, Johannes Gutenberg Universität Mainz, 55128 Mainz, Germany.
2. Helmholtz Institut Mainz, 55128 Mainz, Germany;  
GSI Helmholtzzentrum für Schwerionenforschung, Darmstadt, Germany.
3. Institute for Bioengineering of Catalonia, Barcelona Institute of Science and  
Technology, 08028 Barcelona, Spain.
4. University of California at Berkeley, California 94720-7300, USA.

E-mail: [dbarskiy@uni-mainz.de](mailto:dbarskiy@uni-mainz.de)

## Abstract

Zero- to ultralow-field nuclear magnetic resonance (ZULF NMR) is a rapidly developing form of spectroscopy that drastically reduces the size and expense of portable devices with NMR capabilities. However, signal acquisition still requires a mechanism for orienting nuclear spins (e.g., generating a bulk magnetic moment for detection), and the currently employed methods only apply to a limited pool of chemicals or come at prohibitively high cost. Here, we demonstrate that the parahydrogen-based SABRE-relay method (SABRE = Signal Amplification by Reversible Exchange) can be used as a more general means of generating hyperpolarized analytes for ZULF NMR. This method is applicable to a wide range of small molecules possessing exchangeable protons, as we demonstrate here by observing zero-field  $J$ -spectra of [ $^{13}\text{C}$ ]-methanol, [ $1\text{-}^{13}\text{C}$ ]-ethanol, and [ $2\text{-}^{13}\text{C}$ ]-ethanol. We also explore the magnetic-field dependence of the proton hyperpolarization efficiency in SABRE-relay, and show the existence of a second, previously unexplored maximum at  $19.0 \pm 0.3$  mT. We further demonstrate that water does not significantly diminish SABRE-relay performance using benzylamine as polarization-transfer agent and use this to hyperpolarize ethanol extracted from a store-bought sample of vodka ( $^1\text{H}$  polarization of  $\sim 0.1\%$ ). Applications for detecting trace chemical impurities and measuring  $J$ -coupling spectra from natural extracts are also discussed.

## Teaser

We widen the scope of zero-field NMR by using SABRE-relay-hyperpolarized molecules.

## 3 MAIN TEXT

### 5 Introduction

7 Nuclear magnetic resonance (NMR) is an analytical tool with demonstrated utility across a broad  
8 range of disciplines, from analytical chemistry (1), to medicine (2–4), to fundamental physics (5–  
9 7). Zero- to Ultralow-Field (ZULF) NMR is an emerging NMR modality that can produce rich  
0 spectroscopic information without the need for large magnetic fields (8, 9). This comes with some  
1 advantages over high-field NMR, such as the ability to detect NMR in the presence of conductive  
2 materials (e.g., metals) and in heterogeneous environments without losing spectral resolution (10).  
3 ZULF NMR utilizes non-inductive sensors, typically optically pumped magnetometers (OPMs)  
4 (11), which are highly sensitive (10-20 fT/Hz<sup>1/2</sup>) (12), easy to handle (13), and commercially  
5 available (14); this recent development now makes it straightforward to assemble stand-alone  
6 ZULF NMR spectrometers (15).

8 NMR spectra of molecules at zero field, known as *J*-spectra, arise from heteronuclear *J*-couplings  
9 between spin-active nuclei (16, 17). Solution-state *J*-spectra of molecules containing spin-1/2  
0 heteronuclei appear as groups of peaks with narrow linewidth (0.01-0.5 Hz), at frequencies that  
1 are dependent on the topology of the scalar couplings (*J*-couplings) between the spins. Using the  
2 Pople notation (18), an XA<sub>2</sub> group such as a <sup>13</sup>CH<sub>2</sub> (methylene) group displays one peak at 1.5  
3 *J*<sub>CH</sub> in a *J*-spectrum while an XA<sub>3</sub> group such as a <sup>13</sup>CH<sub>3</sub> (methyl) group displays two peaks: one  
4 at the heteronuclear coupling frequency, *J*<sub>CH</sub>, and the other at twice this value, 2 *J*<sub>CH</sub> (8). Spectra  
5 of more complex molecules containing different types of interacting groups are complicated  
6 further by additional splittings due to multiple bond *J*-couplings between neighboring spins.  
7 Despite their apparent complexity, *J*-spectra offer unique information allowing chemical  
8 identification based on the topology of field-independent scalar coupling between spins, in  
9 contrast to the field-dependent chemical shift differences of high-field NMR, making them akin to  
0 molecular fingerprints (19).

2 An appealing aspect of ZULF NMR is the ability to minimize the size and cost of NMR  
3 spectrometers compared to high-field (including benchtop) counterparts, paving the way for their  
4 use beyond chemical laboratories (15). Despite these advantages, a persistent challenge is still  
5 present in the current iteration of ZULF NMR spectrometers: the system under study must be  
6 externally polarized before the signal can be detected. The “brute-force” approach of allowing a  
7 sample to reach thermal equilibrium polarization in a magnetic field prior to zero-field detection  
8 yields low polarization ( $P_{1H} \sim 10^{-5}$  at 2 T) and is detrimental to portability (20). Furthermore, this  
9 method is mostly limited to concentrated samples and/or large magnetic fields, so alternative  
0 avenues for generating substantial NMR signals are required.

2 Hyperpolarization techniques present an alternative to the brute-force approach, and techniques  
3 such as PHIP (parahydrogen-induced polarization) (21), SABRE (Signal Amplification By  
4 Reversible Exchange) (22–24), and *d*DNP (dissolution Dynamic Nuclear Polarization) (25), have  
5 already been shown to produce sufficient signal for detection in the ZULF regime (26–29).  
6 SABRE is especially well suited for this, since: (i) it is based on chemical interactions of  
7 parahydrogen (*p*H<sub>2</sub>) which can be quickly and inexpensively produced (23); (ii) hyperpolarization  
8 can be generated multiple times in the same sample, allowing multiple experiments signal  
9 averaging; (iii) transfer of polarization from *p*H<sub>2</sub> to heteronuclei such as <sup>15</sup>N and <sup>13</sup>C typically  
0 occurs at fields in the μT regime (0.1 – 1.0 μT for <sup>15</sup>N and <sup>13</sup>C), which is synergistically  
1 compatible with ZULF NMR detection requirements such as shielding from the Earth’s magnetic  
2 field (30, 31).

3  
4 Central to the SABRE technique is an Ir metal complex, referred to as the polarization-transfer  
5 catalyst, that mediates the transfer of nuclear spin order from  $p\text{H}_2$  to a transiently bound substrate.  
6 The scope of substrates that can be hyperpolarized by SABRE is limited by the requirement that  
7 the substrate must reversibly bind and dissociate from the complex on a suitable time scale,  
8 ranging from milliseconds to seconds (32). However, the recent introduction of SABRE-relay has  
9 ameliorated this limitation: polarization is transferred from a carrier molecule (which can be  
0 directly polarized by SABRE) to a secondary substrate through binding of a second metal  
1 complex or through proton exchange (33, 34). In this work we only consider the latter method  
2 (**Figure 1A**). This innovation, along with the even more recent PHIP-X technique (35), has  
3 expanded the pool of polarizable substrates to encompass, in theory, any molecule with  
4 exchangeable protons. Here, we demonstrate that chemical exchange effects (28, 36) do not  
5 inhibit ZULF NMR detection of hyperpolarized, primary alcohols in organic solvent  
6 dichloromethane (DCM), where the polarization is derived from exchangeable protons of the  
7 hydroxyl group.

## 9 **Results**

1 In this work, two NMR detection principles were employed: inductive detection at 1 T or 1.4 T  
2 using benchtop NMR spectrometers, and detection using a commercially available optically  
3 pumped magnetometer (OPM) in ZULF conditions (**Figure 1B**). Benchtop NMR experiments  
4 were performed to optimize the chemical composition of the system and experimental parameters  
5 (e.g.,  $p\text{H}_2$  pressure and flow rate, and polarization-transfer field, etc.) for obtaining maximal  
6 molar polarization, defined as the product of polarization and the concentration of the nuclei  
7 contributing to the signal (37), of methanol and ethanol, see below. ZULF NMR spectra were  
8 recorded on the sample with optimal chemical composition.

### 9 **Detection of SABRE-relay NMR signals from methanol at 1 T**

0 **Figure 1C** illustrates the enhancement of methanol NMR signals via SABRE-relay on a sample  
1 of 230 mM methanol, 230 mM benzylamine, and 12 mM SABRE catalyst (see Materials and  
2 Methods) in DCM.  $p\text{H}_2$  was bubbled through the sample at 4 bar for 10 s in a 7 mT field ( $B_T$ ),  
3 followed by transfer to a 1 T benchtop NMR magnet for the acquisition of the hyperpolarization  
4 enhanced signal. After the signals had fully relaxed, a spectrum was acquired of the sample at  
5 thermal equilibrium polarization. Note that the hyperpolarization enhanced  $^1\text{H}$  NMR signals of  
6 the carrier amine benzylamine ( $\text{BnNH}_2$ ) and methanol are negative. Due to intermolecular proton  
7 exchange between -OH and - $\text{NH}_2$  groups in DCM, their NMR resonances coalesce into a single  
8 broad line.

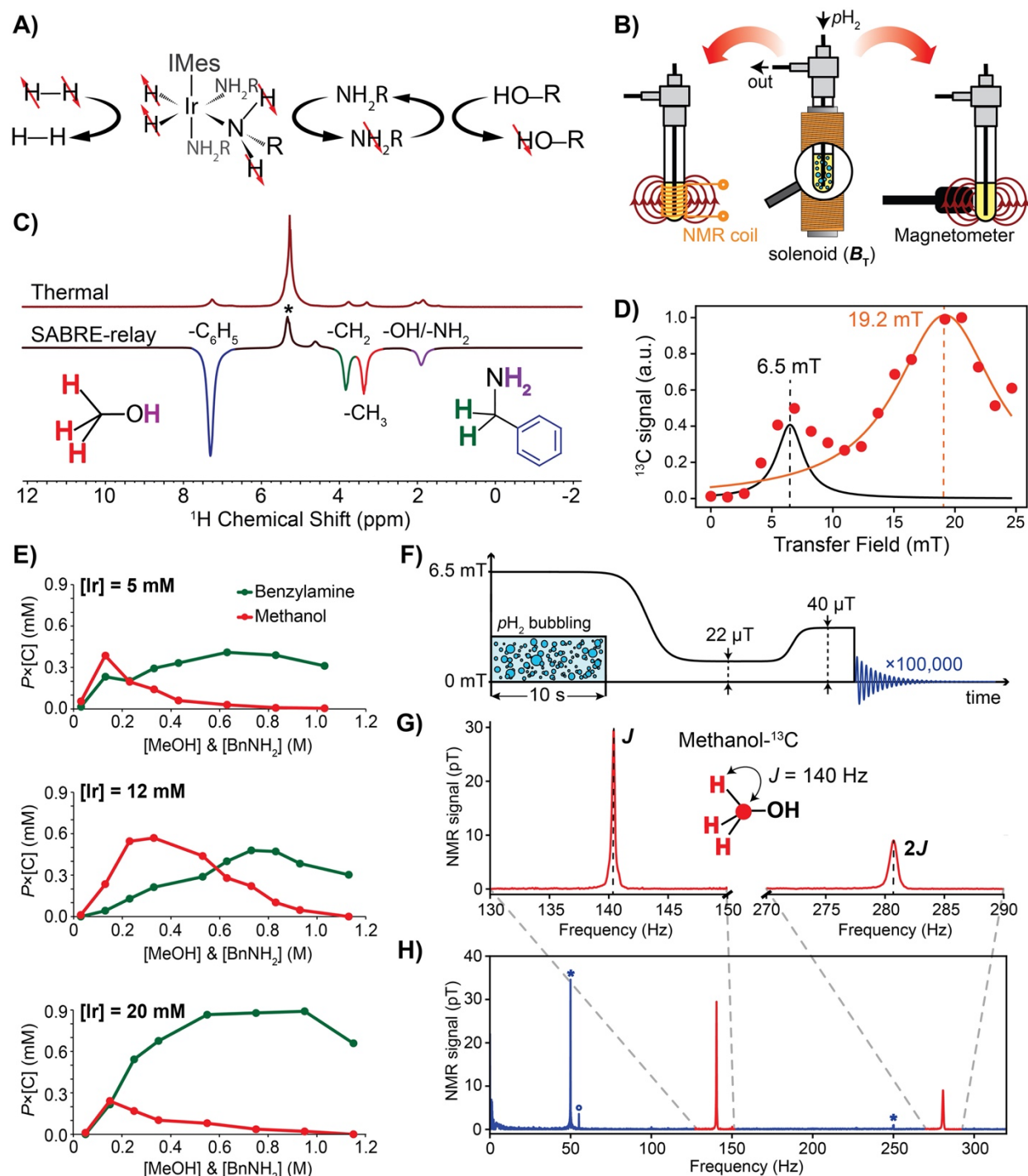


**Figure 1.** A) Molecular diagram of the SABRE-relay process: (i) parahydrogen ( $p\text{H}_2$ ) coordinates with Ir catalyst to form  $[\text{Ir}(\text{IMes})(\text{BnNH}_2)_3\text{H}_2]$ , allowing the transfer of spin order onto the bound substrate, benzylamine ( $\text{BnNH}_2$ ) and, subsequently, to the alcohols via proton exchange. B) Schematic of the SABRE-relay experiment showing two possible detection modes: (**left**) inductive detection employed in this work using a benchtop NMR spectrometer (40 MHz or 60 MHz); and (**right**) detection of NMR with an optically pumped magnetometer in the zero- to ultralow field (ZULF) regime. C)  $^1\text{H}$  NMR spectrum (1.4 T) of methanol and benzylamine (both 230 mM) in DCM at thermal equilibrium polarization (top) compared to a SABRE-relay hyperpolarized ( $B_T \sim 7$  mT) spectrum of the same sample (below). D) Magnetic field dependence of SABRE-relay-derived hyperpolarization of methanol detected via  $^{13}\text{C}$  DEPT at 1.4 T showing two clear maxima. E) Methanol molar polarization optimized as a function of methanol and benzylamine concentrations. Both chemicals were increased in

tandem by adding concentrated stock solution to the activated SABRE catalyst ( $[\text{Ir}(\text{IMes})\text{S}_3\text{H}_2]$ , also denoted  $[\text{Ir}]$ ) at different concentrations. F) ZULF NMR event sequence, showing bubbling of  $p\text{H}_2$  into the sample at 6.5 mT for 10 s followed by a drop in field induced by sample insertion into magnetic shield through the solenoid (22  $\mu\text{T}$ ) before reaching the 40  $\mu\text{T}$  Helmholtz-coil field. This was non-adiabatically switched off immediately prior to acquisition of the NMR signal. G) ZULF NMR spectrum (64 scans) of SABRE-relay-polarized methanol- $^{13}\text{C}$  (230 mM methanol, 230 mM benzylamine, 12 mM  $[\text{Ir}]$ ) showing peaks at  $J$  and  $2J$ , where  $J$  is the heteronuclear  $^1J_{\text{CH}}$  coupling. H) Full ZULF NMR spectrum (64 scans) showing 50 Hz noise peak and overtones from transmission-line noise (\*) and noise arising from the laser of the OPM sensor and the temperature-stabilization circuit (°).

9

## 0 **Field-dependence of SABRE-relay hyperpolarization**

1 To optimize for NMR signal enhancement, SABRE-relay experiments were performed at various  
2 polarization-transfer fields ( $B_{\text{T}}$ ). After a 10 s period of  $p\text{H}_2$  bubbling at  $B_{\text{T}}$ , a sample – containing  
3 benzylamine, methanol, and polarization-transfer catalyst  $[\text{Ir}(\text{IMes})(\text{COD})]\text{Cl}$  ( $[\text{Ir}]$ ), all at natural  
4 isotopic abundance – was transferred to a 1.4 T NMR magnet, and the  $^{13}\text{C}$  signal was detected  
5 after application of a DEPT (Distortionless Enhancement by Polarization Transfer) pulse  
6 sequence (38). Choosing an inter-pulse delay of  $1/(2J)$  in DEPT allowed transferring polarization  
7 from  $^1\text{H}$  to  $^{13}\text{C}$  spins in  $-\text{CH}_3$  groups of methanol. Plotting the  $^{13}\text{C}$  peak integrals as a function of  
8 transfer field and fitting the data with the sum of two Lorentzians revealed two distinct maxima at  
9  $6.5 \pm 0.3$  mT and  $19.2 \pm 0.3$  mT (**Figure 1D**).  $^{13}\text{C}$  NMR signal was used for spectral clarity, due  
0 to overlap of benzylamine and methanol resonances in the  $^1\text{H}$  spectrum.

## 1 **Optimization of methanol $^1\text{H}$ molar polarization**

2 Hyperpolarization derived from SABRE-relay has been shown to be highly dependent on the  
3 concentrations of substrate, carrier amine, and the catalyst, and we verified with experiments  
4 (**Figure S7**) that an equimolar methanol:benzylamine mixture gives the highest methanol  
5 polarization, in accordance with the results from Rayner et al. (39). In order to further increase the  
6 observable signal by optimizing methanol molar polarization the concentrations of methanol and  
7 benzylamine were varied (**Figure 1E**). We observed that increasing the concentrations of both  
8 methanol and benzylamine yielded maximal  $\text{BnNH}_2$  molar polarization at 0.6-0.8 M; higher  
9 SABRE-catalyst concentration gave larger  $\text{BnNH}_2$   $^1\text{H}$  NMR signals. This was not the case for the  
0 molar polarization of methanol, which was larger at a catalyst concentration of 12 mM, resulting  
1 in molar polarization of 0.2 mM at 300 mM (**Figure 1E**).

## 2 **SABRE-relay hyperpolarization of ethanol extracted from vodka**

3 Ethanol was extracted from store-bought vodka (Puschkin, 37.5%) by mixing 1.9 mL of activated  
4 SABRE solution consisting of 230 mM benzylamine and 12 mM  $[\text{Ir}(\text{IMes})(\text{COD})]\text{Cl}$  with 1.9 mL  
5 of vodka (40). The resulting solution was examined in a thermal equilibrium  $^1\text{H}$  NMR experiment  
6 and the ethanol concentration was determined to be 650 mM. A SABRE-relay-enhanced  $^1\text{H}$  NMR  
7 spectrum (1 T) recorded for the same sample after 10 s of  $p\text{H}_2$  bubbling at 6.5 mT shows  
8 significantly enhanced  $^1\text{H}$  resonances of all protons in  $\text{BnNH}_2$  and in ethanol (**Figure 2A**).

## 9 ZULF NMR detection of SABRE-relay hyperpolarized [ $^{13}\text{C}$ ]-methanol

0 ZULF NMR detection of SABRE-relay-polarized, isotopically enriched (99%  $^{13}\text{C}$ ) [ $^{13}\text{C}$ ]-  
1 methanol was performed as follows:  $p\text{H}_2$  was bubbled at 4 bar for 10 s through a solution in a  
2 solenoid ( $B_T = 6.5$  mT) located above the  $\mu$ -metal shielding of the ZULF NMR spectrometer.  
3 After the  $p\text{H}_2$  flow was ceased, the sample was automatically transferred through a guiding  
4 solenoid ( $22$   $\mu\text{T}$ ) to the zero-field region in which a magnetic field of  $40$   $\mu\text{T}$  was being applied in  
5 the direction of the sensitive axis of the magnetometer. This magnetic field was then non-  
6 adiabatically switched off (in  $10$   $\mu\text{s}$ ) to generate an observable signal decay which was picked up  
7 by the magnetometer (**Figure 1F**). Via automation, the sequence could be repeated to accumulate  
8 multiple signal acquisition scans. Fourier transform of the free decay gives ZULF NMR spectra in  
9 which characteristic resonances of [ $^{13}\text{C}$ ]-methanol are observed at  $140.084 \pm 0.001$  Hz and  
0  $280.156 \pm 0.002$  Hz in 64 scans (**Figure 1G**).

1

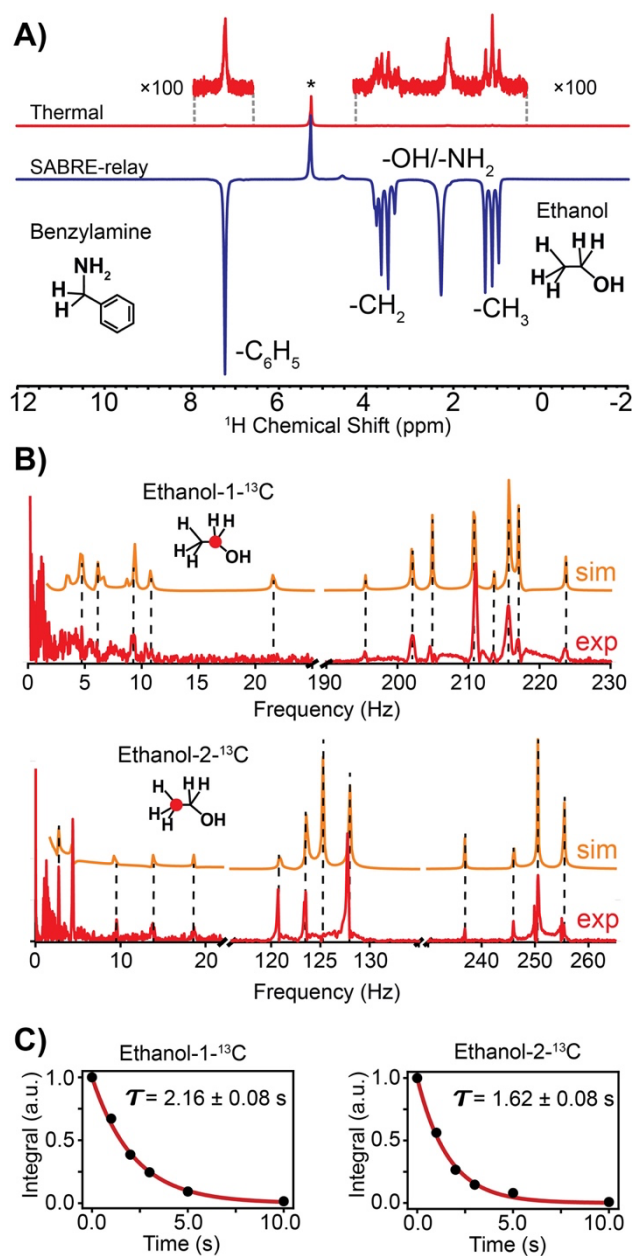


**Figure 2. SABRE-relay of ethanol extracted from vodka sample.** **A)** High-field (1 T) single-scan  $^1\text{H}$  NMR spectra of thermal-equilibrium polarized (top) and single-scan SABRE-relay hyperpolarized (bottom) ethanol extracted from vodka directly into a SABRE solution containing benzylamine and activated Ir catalyst. The final solution consisted of benzylamine (260 mM) and ethanol (650 mM) in dichloromethane with 12 mM  $[\text{Ir}(\text{IMes})(\text{COD})]\text{Cl}$  (and 650 mM extracted  $\text{H}_2\text{O}$  from the vodka sample), showing an enhancement of  $\sim 170$  and polarization of  $\sim 0.1\%$ . **B)** Simulated and experimental zero-field  $J$ -spectra (64 scans) of labeled  $[1\text{-}^{13}\text{C}]$ -ethanol and  $[2\text{-}^{13}\text{C}]$ -ethanol (230 mM) hyperpolarized by SABRE-relay separately using the carrier amine benzylamine; note different scaling in the frequency regions introduced for clarity. Red dots represent the positions of the  $^{13}\text{C}$  nucleus. **C)** Relaxometry of  $[1\text{-}^{13}\text{C}]$ - and  $[2\text{-}^{13}\text{C}]$ -ethanol at zero field obtained by integrating the peaks at 210 and 128 Hz, respectively, and fitting the results with a monoexponential decay function with the stated time constant. Each data point represents the result of four scans.

2

### 3 ZULF NMR detection of SABRE-relay NMR signals from $^{13}\text{C}$ -ethanol

4 The polarization methodology developed for the observation of ZULF NMR signals from  $^{13}\text{C}$ -  
5 methanol was applied to  $^{13}\text{C}$ -ethanol. When  $[1\text{-}^{13}\text{C}]$ -ethanol was used as a SABRE-relay  
6 substrate, two groups of peaks are observed in  $J$ -spectra. The first group of peaks are low-  
7 frequency peaks within the 3-11 Hz region, which arise from the relatively small  $^2J_{\text{CH}}$  coupling.  
8 The second group of peaks are high-frequency peaks with major resonances lying between  
9 200 Hz and 230 Hz, which corresponds to an expected transition at  $(3/2)J_{^{13}\text{C}\ ^1\text{H}} = 211.278$  Hz (  
0  $J_{^{13}\text{C}\ ^1\text{H}} = 140.852 \pm 0.001$  Hz), split by the proton-proton  $J$ -couplings. Experimentally observed  
1 spectra are compared with the results of numerical spin dynamical simulations (see SI for details).  
2 When  $[2\text{-}^{13}\text{C}]$ -ethanol was used as a SABRE-relay substrate, three groups of peaks can be  
3 distinguished. The first group of peaks are low-frequency peaks below 20 Hz. The second group  
4 of peaks are centered around  $J_{^{13}\text{C}\ ^1\text{H}} = 125.257 \pm 0.001$  Hz from the  $\text{CH}_3$  group of ethanol. The  
5 third group of peaks lie between 230 Hz and 260 Hz corresponding to an expected transition  
6 around at  $2J_{^{13}\text{C}\ ^1\text{H}}$ . Experimentally observed spectra are compared with the results of numerical  
7 calculations of spin dynamics (MATLAB code available in SI) starting with equal polarization of  
8 all protons in the molecule. We note that various initial polarization states were employed for  
9 simulations and the results are presented in Supporting Information and discussed further in the  
0 text.

### 1 ZULF NMR relaxometry of hyperpolarization enhanced NMR signals from $^{13}\text{C}$ -ethanol

2 Relaxation of hyperpolarization enhanced ZULF NMR signals of  $[1\text{-}^{13}\text{C}]$ -ethanol (**Figure 2D**)  
3 and  $[2\text{-}^{13}\text{C}]$ -ethanol (**Figure 2E**) was monitored by incrementing a time delay between the sample  
4 arrival to the ZULF region and the beginning of spectral acquisition. Integrating the largest  
5 spectral peaks (at 210 Hz and 250 Hz for  $[1\text{-}^{13}\text{C}]$ -ethanol and  $[2\text{-}^{13}\text{C}]$ -ethanol, respectively) and  
6 fitting the corresponding time traces with monoexponential decay functions gave relaxation time  
7 constants of  $2.16 \pm 0.08$  s and  $1.62 \pm 0.08$  s, respectively. Such short relaxation times are  
8 expected since the  $^1\text{H}$  and  $^{13}\text{C}$  spins are close in space, leading to efficient intramolecular dipole-  
9 dipole relaxation.

0

## 1 Discussion

### 3 Inductive and non-inductive detection of SABRE-relay-enhanced NMR signals

5 The two detection modalities (inductive and non-inductive) demonstrated in **Figure 1B** are  
6 compatible with each other such that the same sample can be used with either modality. A  
7 modular system for  $p\text{H}_2$  sparging and sample shuttling may be switched between the two  
8 modalities on demand within minutes. Using a benchtop NMR system for optimizing SABRE-  
9 relay is advantageous for many reasons, including rapid spectral acquisition, excellent  
0 accessibility, and reproducibility which allows rapid alteration of parameters to maximize  $^1\text{H}$   
1 NMR polarization. This greatly helps to optimize system parameters such as temperature,  
2 concentrations,  $p\text{H}_2$  pressure and flow rate prior to attempting ZULF NMR measurements.

3 We choose molar polarization as a figure of merit for optimization experiments (**Figure 1E**).  
4 Molar polarization is a product of nuclear spin polarization (units of polarization, dimensionless)  
5 and concentration (mol/L). Polarization itself is a good figure of merit for many experiments in  
6 which the hyperpolarized target is produced in similar concentration in each experiment (e.g., as  
7 is often the case with dissolution DNP), or in which the concentration is limited by a biological  
8 process or chemical reaction. However, molar polarization is better suited for cases in which the  
9 largest signal from a fixed-volume sample is desired.

0 The magnetic-field profile used for implementing OPM-based NMR detection is shown in  
1 **Figure 1F**. Parahydrogen was bubbled through a SABRE mixture at 6.5 mT or 19.2 mT (for  
2 polarization buildup) and then mechanically transferred to the zero-field region. Inside an  
3 enclosure made of four layers of  $\mu$ -metal shielding, a solenoid coil provided a 22  $\mu\text{T}$  field  
4 between the shield layers for sample transfer, and an additional Helmholtz coil was placed to  
5 provide a field of 40  $\mu\text{T}$  oriented in the direction of the OPM sensitive axis (located perpendicular  
6 to the long axis of the NMR tube) to be the dominant field at the sample location prior to  
7 detection. This field was then non-adiabatically switched off within 10  $\mu\text{s}$  and the signal was  
8 measured with the QuSpin-Zero Field Magnetometer (QZFM) OPM. In principle, an alternative  
9 detection approach can be successfully used where short pulses of magnetic field can generate  
0 initial coherence for signal detection. We carried out experiments using this pulsed approach, and  
1 the data is presented in Supporting Information **Figure S11**.

2 One should note that while OPMs are used in this work as an example of non-inductive sensors;  
3 other sensors such as SQUIDs, magneto-resistive sensors, or NV-centers in diamonds can be  
4 used; examples of ZULF NMR with such sensors have been demonstrated in the literature (41–  
5 43).

### 6 Mechanism of SABRE-relay polarization transfer via benzylamine

7 The mechanism of polarization transfer to protons in conventional SABRE is generally well  
8 understood. When the  $J$ -coupling value between hydride nuclei ( $J_{\text{HH}} \cong -7$  Hz) in the SABRE  
9 complex matches the Larmor frequency difference between the hydride and bound substrate  
0 spins, singlet spin order of  $p\text{H}_2$  can be converted into observable magnetization of the substrate.  
1 The sign of magnetization depends on the relative sign of the  $J$ -coupling and the frequency  
2 difference. Since such chemical shift difference is similar for a variety of substrates (due to the  
3 large separation of  $\sim 30$  ppm units) and  $J_{\text{HH}}$  is generally independent of the nature of the bound  
4 substrate, the value of the magnetic field, on the order of 6-7 mT (44), optimal for polarization  
5 transfer is virtually the same for all SABRE substrates. In SABRE-relay, the polarization of the  
6

7 protons in an NH<sub>2</sub>-group of benzylamine is transferred to the methanol due to chemical exchange.  
8 This explains the spectrum shown in **Figure 1C** where resonances of -NH<sub>2</sub>, -CH<sub>2</sub>, and benzyl-  
9 groups of BnNH<sub>2</sub> as well as -CH<sub>3</sub> and -OH groups of methanol all demonstrate enhanced emissive  
0 signals. To the best of our knowledge, polarization-transfer field dependence of the SABRE-relay  
1 process for alcohols was never studied at fields above 14 mT (33). The investigated region up to  
2 25 mT revealed the presence of two maxima (**Figure 1D**).  
3

4 The first peak at 6.5 mT is the expected maximum corresponding to the symmetric active SABRE  
5 complex [Ir(IMes)(BnNH<sub>2</sub>)<sub>3</sub>H<sub>2</sub>], **Figure 1A**, and the conventional polarization-transfer  
6 mechanism as described above (45). The nature of the second peak is still under investigation, but  
7 may have two possible explanations. First, this maximum may originate from an asymmetric Ir  
8 complex operating under a mechanism similar to the one described by Emondts et al. This  
9 mechanism, called NEPTUN (Nuclear Exchange Polarization by Transposing Unattached  
0 Nuclei), is based on direct hydride transfer from the catalyst to an axially bound substrate which  
1 has a labile proton (**Figure S12**) (46). This requires formation of an asymmetric complex where  
2 the chemical equivalence of the bound hydrides is broken forming an AB spin system which then  
3 evolves magnetization that can be detected in the substrate following hydride transfer. The second  
4 explanation involves magnetic field dependence complicated by the presence of a heteronucleus,  
5 such as <sup>15</sup>N. Indeed, a single heteronucleus present in the active SABRE complex can split a  
6 single maximum in the magnetic field dependence into two (31, 47). Maximum efficiency of the  
7 NEPTUN effect is predicted when the chemical shift difference between the hydrides in an  
8 asymmetric complex is equal to the *J*-coupling between them. Alternatively, the splitting of the  
9 field maxima for an AA'BX system would depend on the value of  $|J_{AX} - J_{A'X}|$ . Our attempts to  
0 directly observe the hydride resonances indicative of the NEPTUN effect have not been  
1 successful, and the investigation as to whether natural abundance of <sup>15</sup>N nuclei in benzylamine  
2 (~0.36% of naturally occurring nitrogen-15) is enough to cause the observed effect is still  
3 ongoing.  
4

5 It was reported that the presence of water detrimentally effects SABRE-relay efficiency (34). This  
6 is possibly due to the accelerated proton exchange which may affect protons in the carrier amine  
7 during the time it is bound to the complex, thus, altering the spin dynamics (45). Our findings in  
8 the conditions studied show that <sup>1</sup>H NMR signal enhancement of methanol is decreased by a  
9 factor of ~2 after addition of 5 μL of water to 0.5 mL of the SABRE-relay sample with *B<sub>T</sub>* ~ 6 mT  
0 (**Figure S4**). When the second maximum at 19.2 mT in the SABRE-relay field profile was used  
1 for polarization buildup, the presence of water did not significantly alter the intensity of methanol  
2 hyperpolarization. However, studies with ethanol as a substrate revealed an insignificant effect of  
3 the polarization transfer field upon addition of three subsequent 5 μL aliquots of water  
4 (**Figure S4**). The dependence on H<sub>2</sub>O concentration may indirectly support the hypothesis  
5 involving proton exchange since it is the spins from water that are predominantly expected to be  
6 polarized by the NEPTUN effect. However, we note that magnetic field dependence of the  
7 SABRE process of BnNH<sub>2</sub> alone (no methanol added) also revealed the presence of the two  
8 distinct maxima (**Figure S5**). This observation casts doubts that polarization of alcohols in the  
9 conditions tested in this paper is due to direct binding to the complex; further investigations of the  
0 effect of naturally abundant <sup>15</sup>N-nuclei are ongoing, however, these are beyond the scope of this  
1 paper.  
2

### 3 **Zero-field NMR spectroscopy of SABRE-relay-polarized alcohols** 4

5 Experimentally observable ZULF NMR spectra of [<sup>13</sup>C]-methanol and [<sup>13</sup>C]-ethanol match well  
6 with the theoretically calculated spectra (**Figure 2B-C**). On top of the main one-bond

7 heteronuclear  $J$ -coupling, presence of additional  $J$ -couplings between spins from different  
8 chemical groups in ethanol generates a complex spectral pattern which is generally well  
9 reproduced. However, one can see that not all features in  $J$ -spectra are reproduced by the  
0 simulated spectra.

1  
2 While in general the positions of the peaks in experimental  $J$ -spectra match well to the calculated  
3 ones and the ones demonstrated previously (48), the intensity of the lines deviates significantly  
4 from calculations. These deviations in peak amplitude are seen for both [1- $^{13}\text{C}$ ]-ethanol and [2-  
5  $^{13}\text{C}$ ]-ethanol ZULF NMR spectra; they are especially well-pronounced for the latter in the middle  
6 frequency region (for example, note the absence of the peak at 125 Hz in **Figure 2C**). This  
7 transition is well-characterized and corresponds to the flip of carbon-13 spins while the protons in  
8  $-\text{CH}_2-$  group remain in the state with total spin 0. This indicates that the singlet state of the spins  
9 in the  $\text{CH}_2$  group is not overpopulated during the SABRE-relay process and proton magnetization  
0 is a likely starting condition before evolution in the ZULF region.

1  
2 We further investigated this by simulating a variety of ZULF NMR spectra for [1- $^{13}\text{C}$ ]-ethanol  
3 and [2- $^{13}\text{C}$ ]-ethanol starting with different initial proton spin orders (**Figure S2-S3**). Polarization  
4 of all protons as a starting condition was compared to the polarization of protons in  $\text{CH}_3$  and  $\text{CH}_2$   
5 groups separately. While polarization of all  $^1\text{H}$  spin generally fits the experimental observations,  
6 one can see, for example, that a spectral pattern observed for [2- $^{13}\text{C}$ ]-ethanol is reproduced when  
7 polarization of  $\text{CH}_2$  group alone (and not  $\text{CH}_3$  group) is considered. This observation highlights  
8 that protons cannot always be considered strongly coupled at low fields when heteronuclei such  
9 as  $^{13}\text{C}$  are involved in the process. It has been shown recently that heteronuclear spin-spin  
0 interactions suppress the strong coupling regime even when the external field is relatively low  
1 since  $^{13}\text{C}$  spins modify the energy level structure (49). This would mean that SABRE-relay  
2 process via proton exchange, when applied to [2- $^{13}\text{C}$ ]-ethanol at 6.5 mT, would only polarize  
3 proton spins in the  $\text{CH}_2$  group leaving protons in the  $\text{CH}_3$  group unpolarized (or polarized to a  
4 significantly lower degree). The actual experiments involved sample transfer through the near-  
5 zero-field regime before the measurement (**Figure 1F**), thus, partial redistribution of polarization  
6 between all the spins is expected. This may explain the discrepancy between the experimentally  
7 observed spectra and simulations. However, future studies are necessary to understand the exact  
8 nature of polarization transfer during the SABRE-relay process with ZULF NMR measurement,  
9 to obtain the largest signal for the substrate of interest as well as to prepare spin states with  
0 extended lifetimes (such as those found in  $^{-13}\text{CH}_2-$  and  $^{-13}\text{CH}_3$  groups).

## 2 **Hyperpolarization and affordable NMR detection of alcohols from extracted samples**

3  
4 Endowed by relayed polarization transfer via chemical exchange, enhanced benchtop and ZULF  
5 NMR sensing of chemical extracts (e.g. from urine, blood, natural products) is envisioned. As  
6 shown by Tessari *et al* (50), the hydride resonances of the SABRE complexes are sensitive to  
7 different bound substrates, offering a way to detect analytes in exchange with the Ir center which  
8 would otherwise be obscured in complex spectra. In addition, dynamic nuclear polarization  
9 (DNP) has been used to generate large  $^1\text{H}$  and  $^{13}\text{C}$  polarizations of several natural plant extracts as  
0 well as breast-cancer cell extracts (51). Extending this idea to incorporate the use of SABRE-relay  
1 could serve to further increase the analytical potential of high-field and benchtop NMR and make  
2 possible trace analysis of substances using ZULF NMR.

3  
4 While we have not demonstrated ZULF NMR detection of alcohols at mM concentration and  
5 natural  $^{13}\text{C}$  spectroscopic abundance, this is a relatively straightforward task after optimization of  
6 the reaction composition to reduce catalyst deactivation and solvent evaporation.

7  
8 Demonstrated  $^1\text{H}$  polarization levels of 0.1% for ethanol from the store-bought vodka sample  
9 (**Figure 2A**) highlight the analytical potential of the SABRE-relay technique for enhancing  
0 signals from the natural extracts. The advantage of SABRE compared to other hyperpolarization  
1 techniques such as PHIP and *d*DNP lies in the fact that the same sample can be polarized multiple  
2 times by bubbling a fresh portion of  $p\text{H}_2$  gas through the solution and the signal can be averaged  
3 out, increasing the signal-to-noise ratio (SNR). One may note that the intensity of the  $^1\text{H}$  NMR  
4 peak from the solvent is enhanced as is evident from a single-scan SABRE-relay spectrum  
5 compared to the spectrum recorded at thermal equilibrium (**Figure 2A**). We assign this effect to  
6 the intermolecular spin-polarization induced nuclear Overhauser effect (SPINOE) between  
7 hyperpolarized analytes and DCM molecules, which is typical for highly hyperpolarized (e.g.,  
8 magnetized) samples (52).

## 9 0 **Conclusion and future directions**

1  
2 In conclusion, we demonstrate that improving effectiveness of hyperpolarization in the SABRE-  
3 relay methodology enables efficient ZULF NMR measurements of molecules possessing  
4 exchangeable protons. Hyperpolarization of [ $1\text{-}^{13}\text{C}$ ]-methanol, [ $1\text{-}^{13}\text{C}$ ]-ethanol, and [ $2\text{-}^{13}\text{C}$ ]-  
5 ethanol and subsequent ZULF NMR detection of the *J*-spectra of these molecules were  
6 demonstrated and confirmed by numerical simulations. A new maximum in the SABRE field  
7 dependence was discovered which is likely due to the presence of  $^{15}\text{N}$  nuclei at the natural  
8 isotopic abundance in benzylamine. Combination of adiabatic and non-adiabatic field  
9 manipulations with optimal control approaches to effectively simplify the spectra should further  
0 unlock the analytical capabilities of SABRE-relay enhanced ZULF NMR beyond research  
1 laboratories.

## 2 3 **Materials and Methods**

### 4 5 **Optimization**

6  
7 Solutions of methanol, benzylamine and  $[\text{Ir}(\text{COD})(\text{IMes})\text{Cl}]$  ( $[\text{Ir}]$ ) catalyst were prepared in  
8 dichloromethane (DCM, Sigma Aldrich) and hydrogenated at *parahydrogen* ( $p\text{H}_2$ ) pressures from  
9 1 to 6 bar. Hydrogenation was carried out by bubbling the solution with  $p\text{H}_2$  via a 0.9 mm OD  
0 PTFE capillary inserted into a pressurizable 5 mm OD NMR tube fitted with a modified Young's  
1 valve cap. Flow of  $p\text{H}_2$  was controlled by a mass flow controller (Sierra instruments SmartTrack  
2 100) generally set between 20 scc/m (for activation of the polarization transfer catalyst,  $[\text{Ir}]$ ) and  
3 up to 90 scc/m for SABRE-relay experiments, while pressure in the system was controlled via  
4 back pressure regulator (Swagelok). Spectra were recorded in a 1.4 T SpinSolve benchtop  
5 spectrometer (Magritek) for optimization of reaction parameters. Timing of bubbling was  
6 controlled electronically via an Arduino Uno, which was also used to initiate NMR spectral  
7 acquisition. The adjustable SABRE transfer field was provided by a hand-wound solenoid (up to  
8  $\sim 22$  mT) and a custom built variable Halbach array of transversely oriented magnets capable of  
9 generating a field from 1 mT – 101 mT.

0  
1 For concentration-based optimization studies, a stock solution was added stepwise to increase the  
2 concentrations of benzylamine and methanol. We began by adjusting the concentration of  
3 benzylamine while maintaining a methanol concentration of 30 mM by adding 10  $\mu\text{L}$  of a  
4 concentrated benzylamine stock directly to the sample to increase benzylamine concentration in  
5 steps of 20 mM from 10 mM to 110 mM (sample volume, 500  $\mu\text{L}$ ). We repeated the same  
6 procedure for methanol while holding benzylamine concentration at 30 mM and found that a 1:1

7 ratio provided the optimum methanol molar polarization, which we define as the substrate  
8 concentration times its polarization, supporting optimization work done by  
9 Samples were shuttled either by hand or by a robotic arm fitted with a 3D printed adapter to hold  
0 the  $pH_2$  bubbling apparatus.

## 2 **Zero- to Ultralow-Field NMR**

4 Measurements were made using a commercially available optically-pumped magnetometer  
5 (QuSpin) inserted into a Helmholtz array with two orthogonal coils used to generate pulses.  
6 External magnetic fields were blocked by an MS-1  $\mu$ -metal shield from Twinleaf and shimming  
7 of any interior residual field was conducted using built-in shimming coils. Polarization was  
8 generated by bubbling in a 6 mT – 20 mT field generated by an axially-oriented solenoid placed  
9 above the shield, then the sample was plunged into the sensor region using an automated robotic  
0 setup (results will be published elsewhere); variable static field was applied to control the  
1 efficiency of spin order transfer in the SABRE-relay process.

## 3 **References**

- 5 1. P. Giraudeau, Challenges and perspectives in quantitative NMR. *Magn. Reson. Chem.* **55**,  
6 61–69 (2017).
- 7 2. E. Cavallari, C. Carrera, S. Aime, F. Reineri, Metabolic Studies of Tumor Cells Using [1-  
8  $^{13}C$ ] Pyruvate Hyperpolarized by Means of PHIP-Side Arm Hydrogenation.  
9 *ChemPhysChem.* **20**, 318–325 (2019).
- 0 3. P. J. Basser, D. K. Jones, Diffusion-tensor MRI: theory, experimental design and data  
1 analysis - a technical review. *NMR Biomed.* **15**, 456–467 (2002).
- 2 4. R. Damadian, M. Goldsmith, L. Minkoff, NMR in cancer: XVI. FONAR image of the live  
3 human body. *Physiol. Chem. Phys.* **9**, 97–100, 108 (1977).
- 4 5. J. Eills, J. W. Blanchard, L. Bougas, M. G. Kozlov, A. Pines, D. Budker, Measuring  
5 molecular parity nonconservation using nuclear-magnetic-resonance spectroscopy. *Phys.*  
6 *Rev. A.* **96** (2017), doi:10.1103/PhysRevA.96.042119.
- 7 6. A. L. Barra, J. B. Robert, Parity non-conservation and NMR parameters. *Mol. Phys.* **88**,  
8 875–886 (1996).
- 9 7. V. Weijo, P. Manninen, J. Vaara, Perturbational calculations of parity-violating effects in  
0 nuclear-magnetic-resonance parameters. *J. Chem. Phys.* **123** (2005),  
1 doi:10.1063/1.1961321.
- 2 8. J. W. Blanchard, D. Budker, A. Trabesinger, Lower than low: Perspectives on zero- to  
3 ultralow-field nuclear magnetic resonance. *J. Magn. Reson.* **323**, 106886 (2021).
- 4 9. J. W. Blanchard, D. Budker, Zero- to Ultralow-Field NMR. *eMagRes.* **5**, 1395–1410  
5 (2016).
- 6 10. D. B. Burueva, J. Eills, J. W. Blanchard, A. Garcon, R. Picazo-Frutos, K. V. Kovtunov, I.  
7 V. Koptuyug, D. Budker, Chemical Reaction Monitoring using Zero-Field Nuclear  
8 Magnetic Resonance Enables Study of Heterogeneous Samples in Metal Containers.  
9 *Angew. Chemie Int. Ed.* **59**, 17026–17032 (2020).
- 0 11. D. Budker, M. Romalis, Optical magnetometry. *Nat. Phys.* **3**, 227–234 (2007).
- 1 12. M. C. D. Tayler, T. Theis, T. F. Sjolander, J. W. Blanchard, A. Kentner, S. Pustelny, A.  
2 Pines, D. Budker, Instrumentation for nuclear magnetic resonance in zero and ultralow  
3 magnetic field (2017), doi:10.1063/1.5003347.
- 4 13. E. Boto, N. Holmes, J. Leggett, G. Roberts, V. Shah, S. S. Meyer, L. D. Muñoz, K. J.  
5 Mullinger, T. M. Tierney, S. Bestmann, G. R. Barnes, R. Bowtell, M. J. Brookes, Moving  
6 magnetoencephalography towards real-world applications with a wearable system. *Nature.*

- 7 **555**, 657–661 (2018).
- 8 14. J. W. Blanchard, T. Wu, J. Eills, Y. Hu, D. Budker, Zero- to ultralow-field nuclear  
9 magnetic resonance *J*-spectroscopy with commercial atomic magnetometers. *J. Magn.*  
0 *Reson.* **314** (2020), doi:10.1016/j.jmr.2020.106723.
- 1 15. D. A. Barskiy, P. Put, S. Pustelny, D. Budker, E. Druga, T. F. Sjolander, A. Pines, Zero- To  
2 ultralow-field NMR spectroscopy of small biomolecules. *Anal. Chem.* **93**, 3226–3232  
3 (2021).
- 4 16. M. C. Butler, M. P. Ledbetter, T. Theis, J. W. Blanchard, D. Budker, A. Pines, Multiplets  
5 at zero magnetic field: The geometry of zero-field NMR. *J. Chem. Phys.* **138**, 184202  
6 (2013).
- 7 17. T. Theis, J. W. Blanchard, M. C. Butler, M. P. Ledbetter, D. Budker, A. Pines, Chemical  
8 analysis using *J*-coupling multiplets in zero-field NMR. *Chem. Phys. Lett.* **580**, 160–165  
9 (2013).
- 0 18. H. J. Bernstein, J. A. Pople, W. G. Schneider, The analysis of nuclear magnetic resonance  
1 spectra: I. Systems of two and three nuclei. *Can. J. Chem.* **35**, 67–83 (1957).
- 2 19. J. W. Blanchard, M. P. Ledbetter, T. Theis, M. C. Butler, D. Budker, A. Pines, High-  
3 Resolution Zero-Field NMR *J*-Spectroscopy of Aromatic Compounds. *J. Am. Chem. Soc.*  
4 **135**, 3607–3612 (2013).
- 5 20. M. L. Hirsch, N. Kalechofsky, A. Belzer, M. Rosay, J. G. Kempf, Brute-Force  
6 Hyperpolarization for NMR and MRI. *J. Am. Chem. Soc.* **137**, 8428–8434 (2015).
- 7 21. C. R. Bowers, D. P. Weitekamp, Parahydrogen and synthesis allow dramatically enhanced  
8 nuclear alignment. *J. Am. Chem. Soc.* **109**, 5541–5542 (1987).
- 9 22. K. D. Atkinson, M. J. Cowley, P. I. P. Elliott, S. B. Duckett, G. G. R. Green, J. López-  
0 Serrano, A. C. Whitwood, Spontaneous transfer of Parahydrogen derived spin order to  
1 pyridine at low magnetic field. *J. Am. Chem. Soc.* **131**, 13362–13368 (2009).
- 2 23. R. W. Adams, J. A. Aguilar, K. D. Atkinson, M. J. Cowley, P. I. P. Elliott, S. B. Duckett,  
3 G. G. R. Green, I. G. Khazal, J. Lopez-Serrano, D. C. Williamson, Reversible interactions  
4 with para-hydrogen enhance NMR sensitivity by polarization transfer. *Science (80-. )*. **323**,  
5 1708–1711 (2009).
- 6 24. R. W. Adams, S. B. Duckett, R. A. Green, D. C. Williamson, G. G. R. Green, A theoretical  
7 basis for spontaneous polarization transfer in non-hydrogenative parahydrogen-induced  
8 polarization. *J. Chem. Phys.* **131** (2009), doi:10.1063/1.3254386.
- 9 25. J. H. Ardenkjaer-Larsen, B. Fridlund, A. Gram, G. Hansson, L. Hansson, M. H. Lerche, R.  
0 Servin, M. Thaning, K. Golman, Increase in signal-to-noise ratio of > 10,000 times in  
1 liquid-state NMR. *Proc. Natl. Acad. Sci.* **100**, 10158–10163 (2003).
- 2 26. T. Theis, P. Ganssle, G. Kervern, S. Knappe, J. Kitching, M. P. Ledbetter, D. Budker, A.  
3 Pines, Parahydrogen-enhanced zero-field nuclear magnetic resonance. *Nat. Phys.* **7**, 571–  
4 575 (2011).
- 5 27. J. W. Blanchard, B. Ripka, B. A. Suslick, D. Gelevski, T. Wu, K. Münnemann, D. A.  
6 Barskiy, D. Budker, Towards large-scale steady-state enhanced nuclear magnetization with  
7 in situ detection. *Magn. Reson. Chem.* **59**, 1208–1215 (2021).
- 8 28. D. A. Barskiy, M. C. D. Tayler, I. Marco-Rius, J. Kurhanewicz, D. B. Vigneron, S.  
9 Cikrikci, A. Aydogdu, M. Reh, A. N. Pravdivtsev, J. B. Hövener, J. W. Blanchard, T. Wu,  
0 D. Budker, A. Pines, Zero-field nuclear magnetic resonance of chemically exchanging  
1 systems. *Nat. Commun.* **10** (2019), doi:10.1038/s41467-019-10787-9.
- 2 29. R. Picazo-Frutos, Q. Stern, J. W. Blanchard, O. Cala, M. Ceillier, S. F. Cousin, J. Eills, S.  
3 J. Elliott, S. Jannin, D. Budker, “Dissolution Dynamic Nuclear Polarization-Enhanced  
4 Zero-to Ultralow-Field Nuclear Magnetic Resonance” (2022), , doi:10.26434/chemrxiv-  
5 2022-f8t03.
- 6 30. T. Theis, M. L. Truong, A. M. Coffey, R. V. Shchepin, K. W. Waddell, F. Shi, B. M.

- 7 Goodson, W. S. Warren, E. Y. Chekmenev, Microtesla SABRE enables 10% nitrogen-15  
8 nuclear Spin polarization. *J. Am. Chem. Soc.* **137**, 1404–1407 (2015).
- 9 31. D. A. Barskiy, S. Knecht, A. V. Yurkovskaya, K. L. Ivanov, SABRE: Chemical kinetics  
0 and spin dynamics of the formation of hyperpolarization. *Prog. Nucl. Magn. Reson.*  
1 *Spectrosc.* **114–115** (2019), pp. 33–70.
- 2 32. M. J. Cowley, R. W. Adams, K. D. Atkinson, M. C. R. Cockett, S. B. Duckett, G. G. R.  
3 Green, J. A. B. Lohman, R. Kerssebaum, D. Kilgour, R. E. Mewis, Iridium N-heterocyclic  
4 carbene complexes as efficient catalysts for magnetization transfer from para -hydrogen. *J.*  
5 *Am. Chem. Soc.* **133**, 6134–6137 (2011).
- 6 33. S. S. Roy, K. M. Appleby, E. J. Fear, S. B. Duckett, SABRE-Relay: A Versatile Route to  
7 Hyperpolarization. *J. Phys. Chem. Lett.* **9**, 1112–1117 (2018).
- 8 34. W. Iali, P. J. Rayner, S. B. Duckett, Using parahydrogen to hyperpolarize amines, amides,  
9 carboxylic acids, alcohols, phosphates, and carbonates. *Sci. Adv.* **4** (2018),  
0 doi:10.1126/sciadv.aao6250.
- 1 35. K. Them, F. Ellermann, A. N. Pravdivtsev, O. G. Salnikov, I. V. Skovpin, I. V. Koptuyg,  
2 R. Herges, J. B. Hövener, Parahydrogen-Induced Polarization Relayed via Proton  
3 Exchange. *J. Am. Chem. Soc.* **143**, 13694–13700 (2021).
- 4 36. S. Alcicek, P. Put, D. Barskiy, V. Kontul, S. Pustelny, Zero-Field NMR of Urea: Spin-  
5 Topology Engineering by Chemical Exchange. *J. Phys. Chem. Lett.* **12**, 10671–10676  
6 (2021).
- 7 37. S. Knecht, J. W. Blanchard, D. Barskiy, E. Cavallari, L. Dagys, E. Van Dyke, M.  
8 Tsukanov, B. Bliemel, K. Münnemann, S. Aime, F. Reineri, M. H. Levitt E □, G.  
9 Buntkowsky, A. Pines, P. Blümler, D. Budker, J. Eills, C. R. Bowers, M. S. Rosen, F.  
0 Schilling, D. Barskiy, J. E. Designed, J. E. Performed, D. Budker, Rapid hyperpolarization  
1 and purification of the metabolite fumarate in aqueous solution. **118**, 2025383118 (2021).
- 2 38. D. M. Doddrell, D. T. Pegg, M. R. Bendall, Distortionless enhancement of NMR signals by  
3 polarization transfer. *J. Magn. Reson.* **48**, 323–327 (1982).
- 4 39. P. J. Rayner, B. J. Tickner, W. Iali, M. Fekete, A. D. Robinson, S. B. Duckett, Relayed  
5 hyperpolarization from para-hydrogen improves the NMR detectability of alcohols †.  
6 *Chem. Sci.* **10** (2019), doi:10.15124/db5b8475-8c71-4714-95f7-eb5e2a49632c.
- 7 40. F. Ruiz, V. Gomis, R. F. Botella, Extraction of ethanol from aqueous solution. 2. A solvent  
8 more volatile than ethanol: dichloromethane. *Ind. Eng. Chem. Res.* **27**, 648–650 (1988).
- 9 41. A. H. Trabesinger, R. McDermott, S. Lee, M. Mück, J. Clarke, A. Pines, SQUID-Detected  
0 Liquid State NMR in Microtesla Fields. *J. Phys. Chem. A.* **108**, 957–963 (2004).
- 1 42. F. Verpillat, M. P. Ledbetter, S. Xu, D. J. Michalak, C. Hilty, L.-S. Bouchard, S.  
2 Antonijeivic, D. Budker, A. Pines, Remote detection of nuclear magnetic resonance with an  
3 anisotropic magnetoresistive sensor. *Proc. Natl. Acad. Sci.* **105**, 2271–2273 (2008).
- 4 43. H. Zheng, J. Xu, G. Z. Iwata, T. Lenz, J. Michl, B. Yavkin, K. Nakamura, H. Sumiya, T.  
5 Ohshima, J. Isoya, J. Wrachtrup, A. Wickenbrock, D. Budker, Zero-Field Magnetometry  
6 Based on Nitrogen-Vacancy Ensembles in Diamond. *Phys. Rev. Appl.* **11** (2019),  
7 doi:10.1103/PhysRevApplied.11.064068.
- 8 44. E. B. Dücker, L. T. Kuhn, K. Münnemann, C. Griesinger, Similarity of SABRE field  
9 dependence in chemically different substrates. *J. Magn. Reson.* **214**, 159–165 (2012).
- 0 45. S. Knecht, D. A. Barskiy, G. Buntkowsky, K. L. Ivanov, Theoretical description of  
1 hyperpolarization formation in the SABRE-relay method. *J. Chem. Phys.* **153** (2020),  
2 doi:10.1063/5.0023308.
- 3 46. M. Emondts, D. Schikowski, J. Klankermayer, P. P. M. Schleker, Non-Pairwise  
4 Interactions in Parahydrogen Experiments: Nuclear Exchange of Single Protons Enables  
5 Bulk Water Hyperpolarization. *ChemPhysChem.* **19**, 2614–2620 (2018).
- 6 47. A. N. Pravdivtsev, K. L. Ivanov, A. V. Yurkovskaya, P. A. Petrov, H. H. Limbach, R.

- 7 Kaptein, H. M. Vieth, Spin polarization transfer mechanisms of SABRE: A magnetic field  
8 dependent study. *J. Magn. Reson.* **261**, 73–82 (2015).
- 9 48. T. F. Sjolander, J. W. Blanchard, D. Budker, A. Pines, Two-dimensional single- and  
0 multiple-quantum correlation spectroscopy in zero-field nuclear magnetic resonance. *J.*  
1 *Magn. Reson.* **318**, 106781 (2020).
- 2 49. I. V. Zhukov, A. S. Kiryutin, Z. Wang, M. Zachrdla, A. V. Yurkovskaya, K. L. Ivanov, F.  
3 Ferrage, Surprising absence of strong homonuclear coupling at low magnetic field explored  
4 by two-field nuclear magnetic resonance spectroscopy. *Magn. Reson.* **1**, 237–246 (2020).
- 5 50. N. K. J. Hermkens, N. Eshuis, B. J. A. van Weerdenburg, M. C. Feiters, F. P. J. T. Rutjes,  
6 S. S. Wijmenga, M. Tessari, NMR-Based Chemosensing via  $p$ - $H_2$  Hyperpolarization:  
7 Application to Natural Extracts. *Anal. Chem.* **88**, 3406–3412 (2016).
- 8 51. J. N. Dumez, J. Milani, B. Vuichoud, A. Bornet, J. Lalande-Martin, I. Tea, M. Yon, M.  
9 Maucourt, C. Deborde, A. Moing, L. Frydman, G. Bodenhausen, S. Jannin, P. Giraudeau,  
0 Hyperpolarized NMR of plant and cancer cell extracts at natural abundance. *Analyst.* **140**,  
1 5860–5863 (2015).
- 2 52. T. R. Eichhorn, A. J. Parker, F. Josten, C. Müller, J. Scheuer, J. M. Steiner, M. Gierse, J.  
3 Handwerker, M. Keim, S. Lucas, M. U. Qureshi, A. Marshall, A. Salhov, Y. Quan, J.  
4 Binder, K. D. Jahnke, P. Neumann, S. Knecht, J. W. Blanchard, M. B. Plenio, F. Jelezko,  
5 L. Emsley, C. C. Vassiliou, P. Hautle, I. Schwartz, Hyperpolarized Solution-State NMR  
6 Spectroscopy with Optically Polarized Crystals. *J. Am. Chem. Soc.* **144**, 2511–2519 (2022).
- 7  
8

## 9 Acknowledgments

0  
1 We greatly appreciate Dr. Peter Blümler for the construction of “Barskiy-Eills” magnet  
2 capable of providing a variable field in the range of 1-101 mT depending on the relative  
3 angle between two enclosed Halbach magnets.

## 4 Funding:

5 Alexander von Humboldt Foundation in the framework of the Sofja Kovalevskaja Award;  
6 German Research Foundation grant BU 3035/15-1;  
7 European Union's Horizon 2020 research and innovation program under the Marie  
8 Skłodowska-Curie grant agreement No. 766402.

## 9 Author contributions:

0 Conceptualization: DAB

1 Methodology: ETVD, JE, RPF, KFS, YH, DAB

2 Investigation: ETVD, JE, RPF, KFS, DAB

3 Supervision: DB, DAB

4 Writing—original draft: ETVD, DAB

5 Writing—review & editing: ETVD, JE, RPF, KFS, YH, DB, DAB

6  
7  
8  
9 **Competing interests:** Authors declare that they have no competing interests.

0  
1 **Data and materials availability:** All data are available in the main text or the  
2 supplementary materials.  
3

## 4 Supplementary Materials

5

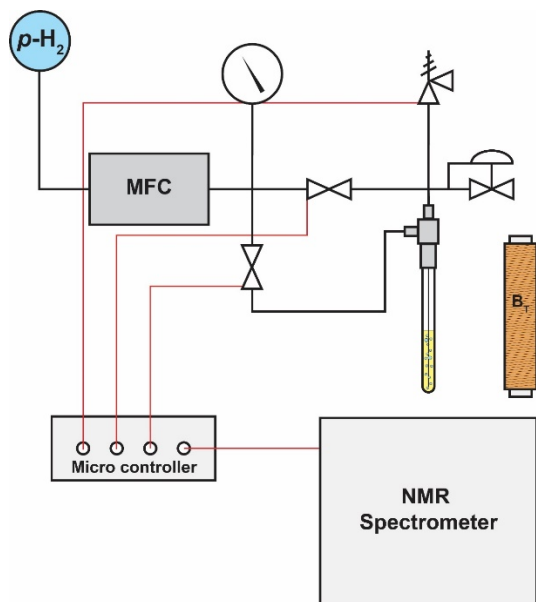


**Figure S1.** Schematic of the experimental control used in SABRE-relay experiments. The microcontroller (MCU), Arduino UNO, controls relays to independently switch on and off three valves used to control the flow of  $p\text{H}_2$  gas: (1) by-pass reaction chamber, (2) stop the inlet flow, (3) release the pressure. The MCU was also used to trigger spectral acquisition via a TTL board (FTDI-UM232H) which communicated with the SpinSolve with a  $\sim 300$  ms delay. Pressure of  $p\text{H}_2$  was maintained via backpressure regulator and flow was controlled by a mass flow controller (MFC), Sierra Instruments. The spectrometers used were either a 60 MHz Carbon SpinSolve or a 43 MHz SpinSolve Nitrogen Ultra (Magritek).

5

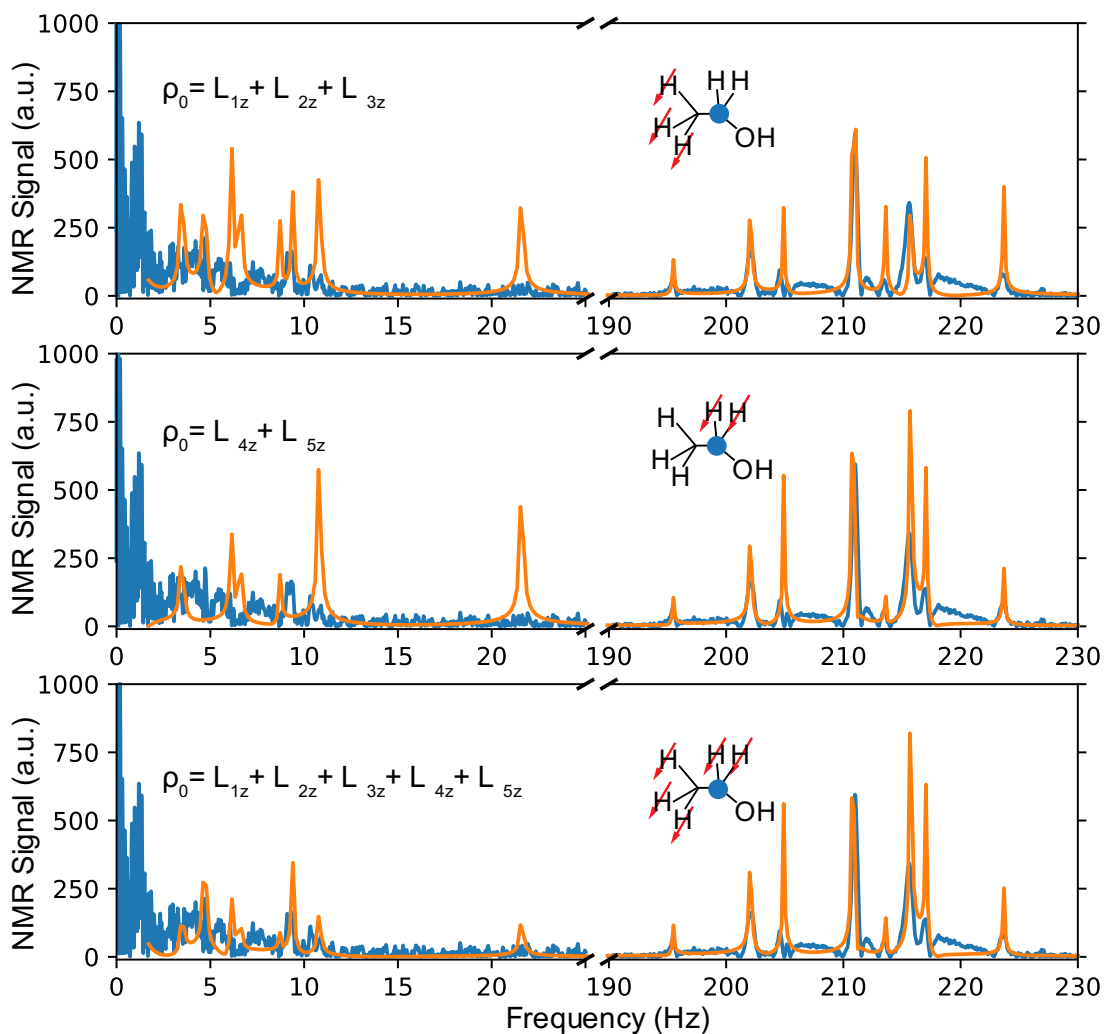


**Figure S2.** Experimentally measured ZULF NMR spectrum (blue) of [1-<sup>13</sup>C]-ethanol hyperpolarized by SABRE-relay using the protocol depicted in Fig. 1F overlaid with three simulated spectra. For the simulated spectra, we varied initial proton polarization: CH<sub>3</sub> group (**top**), CH<sub>2</sub> group (**middle**) and all protons (**bottom**).

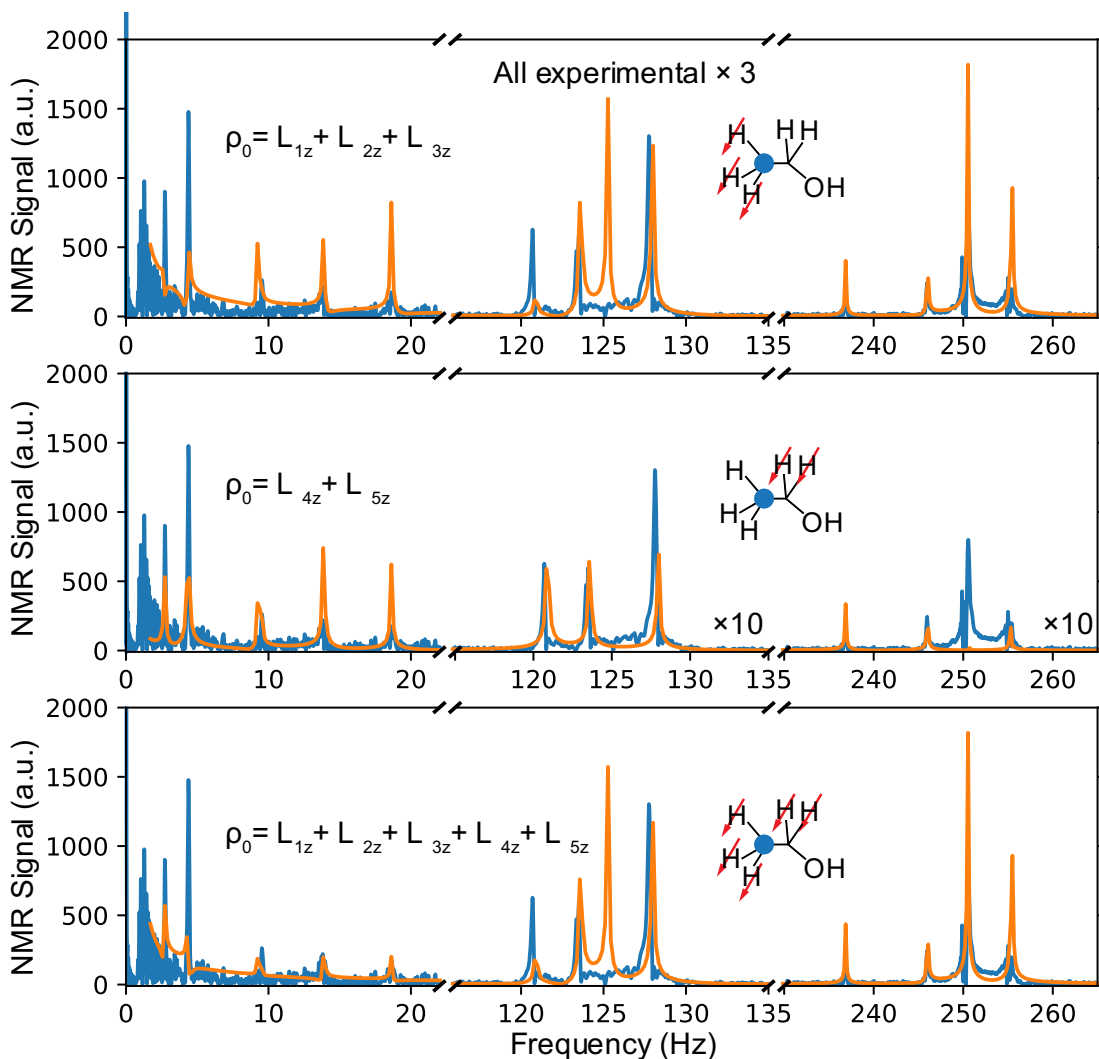


**Figure S3.** Experimentally measured ZULF NMR spectrum (blue) of [2-<sup>13</sup>C]-ethanol hyperpolarized by SABRE-relay using the protocol depicted in Figure 1F overlaid with three simulated spectra. For the simulated spectra, we varied initial proton polarization: CH<sub>3</sub> group (**top**), CH<sub>2</sub> group (**middle**) and all protons (**bottom**). Note that intensity of the experimental spectrum is scaled by a factor 3 compared to the Figure S2 and scaling of parts of the simulated spectra is shown individually.

### MATLAB zero-field simulations

Numerical simulations of the zero field NMR spectra were performed in a manner previously described in the literature based on the *J*-coupling values published by Sjolander et. al (15, 53).

% ZULF Spectrum of ethanol (simplified SABRE-relay process)

% Magnetic field and spectral parameters

B0 = 1e-9; % detection field (T)

```

8   Bandwidth = 700; % range of the full spectrum [Hz] (spectral bandwidth), it is defining
9   the time_step of the evolution
0   FWHH = 0.08; % peaks full width at half height in Hz
1
2   % Parameters of ethanol-1-13C
3   % Substrate parameters
4   ppm_substrate = [1.2 1.2 1.2 3.8 3.8 2.1 60]; % data for ethanol;
5   types_substrate = [0.5 0.5 0.5 0.5 0.5 0.5];
6   N = numel(types_substrate);
7   J1 = 0; J2 = -4.7; J3 = 0; J4 = 0.5; J5 = 140.852; J6 = 0; J7 = 7.049; J8 = 0;
8   J_couplings_substrate = [
9       0 J1 J1 J7 J7 J8 J2;
0       0 0 J1 J7 J7 J8 J2;
1       0 0 0 J7 J7 J8 J2;
2       0 0 0 0 J3 J4 J5;
3       0 0 0 0 0 J4 J5;
4       0 0 0 0 0 0 J6;
5       0 0 0 0 0 0 0;
6       ];
7
8   % Hamiltonian of the substrate in the transfer field
9   [Lx, Ly, Lz] = Spin_Operator_2(types_substrate);
0   H_ZULF = zeros(2^N,2^N);
1
2   %gyromagtenic ratios
3   g_13C = 6728.28; %in units of [rad.s^(-1)/Gauss]
4   g_1H = 26752.22; %in units of [rad.s^(-1)/Gauss]
5
6   % Zeeman terms
7   for i=1:(N-1)
8   H_ZULF = H_ZULF - B0*g_1H*(1+ppm_substrate(i)*1e-6)*Lz{i};
9   end
0
1   H_ZULF = H_ZULF - B0*g_13C*(1+ppm_substrate(7)*1e-6)*Lz{7};
2
3   % Scalar couplings
4   for n=1:N
5       for k=1:N
6           H_ZULF = H_ZULF +
7           2*pi*(J_couplings_substrate(n,k))*(Lx{n}*Lx{k}+Ly{n}*Ly{k}+Lz{n}*Lz{k});
8       end
9   end
0
1   % rho_123 = (1/8)*eye(8);
2   % rho_4 = blkdiag(0.5, -0.5); % initial state (polarization of -OH group)
3   % rho_5 = 0.5*eye(2);
4
5   % rho_0 = Lz{1} + Lz{2} + Lz {3} + Lz{4} + Lz{5} + Lz{6} + Lz{7};
6   % rho_0 = a1*Lz{1} + a2*Lz{2} + a3*Lz{3} + a4*Lz{4} + a5*Lz{5} + a6*Lz{6} +
7   a7*Lz{7};

```

```

8 rho_0 = Lz{1} + Lz{2} + Lz{3} + Lz{4} + Lz{5} + Lz{6} + Lz{7};
9 rho = rho_0;
0
1 % IMPORTANT! Field sweep step down
2 time_sweep = 3; % sweep time [s]
3 time_Bt = 0:1e-3:3;
4 Bt = 6*1e-3*exp(-10*time_Bt);
5 for j=1:numel(Bt)
6     % Computing Hamiltonian for each time step of the field sweep
7     % Zeeman terms
8     H_sweep = zeros(2^N,2^N);
9     for i=1:(N-1)
0         H_sweep = H_sweep - Bt(j)*g_1H*(1+ppm_substrate(i)*1e-6)*Lz{i};
1     end
2
3     H_sweep = H_sweep - Bt(j)*g_13C*(1+ppm_substrate(7)*1e-6)*Lz{7};
4
5     % Scalar couplings
6     for n=1:N
7         for k=1:N
8             H_sweep = H_sweep +
9 2*pi*(J_couplings_substrate(n,k))*(Lx{n}*Lx{k}+Ly{n}*Ly{k}+Lz{n}*Lz{k});
0         end
1     end
2     P_sweep = expm(-1i*H_sweep*time_sweep);
3     rho = P_sweep*rho*(P_sweep');
4 end
5
6 % IMPORTANT! Field sweep step up
7 %
8 %
9 %
0
1 % Simulation: evolution and measurement
2 time_step = 1/(Bandwidth);
3 P_evol = expm(-1i*H_ZULF*time_step);
4 %P_evol=P_evol.*(abs(P_evol)>1e-6); % Clean up Propagator
5
6 P_meas = (g_1H*(Lz{1} + Lz{2} + Lz{3} + Lz{4} + Lz{5} + Lz{6}) +
7 g_13C*Lz{7})/g_1H;
8
9 % Collecting Free Decay (along Z axis)
0 nsteps = 2^(12); % number of steps in the simulation
1 FD = zeros(nsteps,1); % preallocate the array
2 for n=1:nsteps
3     FD(n)
4     = real(trace(P_meas*rho));
5     rho=P_evol*rho*P_evol';
6 end
7

```

```

8     FD_time = nsteps*time_step; % time of FD recording (s)
9
0     % Apodization
1     time=0:time_step:FD_time-time_step;
2     window_function=exp(-(FWHH*pi)*time)';
3     FD = FD.*window_function;
4
5     %High-pass filter
6     FD = highpass(FD, 1, Bandwidth);
7
8     % Fourier transform with zerofilling
9     SI=2^12;
0     % spectrum_Re = real(fftshift(fft(FD, SI))); %(1/SI)
1     % spectrum_Im = imag(fftshift(fft(FD, SI))); %(1/SI)
2     % phase1 = 0;%-pi/2;
3     % phase2 = 0;
4
5     % Frequency axis calibration
6     %x=-Bandwidth/2:Bandwidth/SI:Bandwidth/2-1/SI;
7     x=(1/SI:Bandwidth/SI:Bandwidth/2)';
8     %ZULF_spectrum = spectrum_Re(end/2+1:end).*cos(phase1) -
9     spectrum_Im(end/2+1:end).*sin(phase1);
0     ZULF_spectrum_magn = abs(fftshift(fft(FD, SI)));
1
2     % Plotting
3     %figure;
4
5     % ppm_title=ppm_ref+x*1e+6/v0_HF;
6     % plot(ppm_title,spectrum);
7     % set(gca,'XDir','reverse');
8     % title('Spectrum');
9     % ylabel('Signal, a.u.');
```

```

0     % xlabel('1H chemical shift, ppm');
1
2     %Hz_title=x;
3
4     %time = 0:time_step:(nsteps-1)*time_step;
5
6     %plot(time, spectrum_Re, time, spectrum_Im);
7     plot(x(11:end), ZULF_spectrum_magn(end/2+11:end)); hold on;
8     %plot(Hz_title, S);
9     %xlabel('Frequency, Hz');
```

```

0
1
2     ethZULF = load('Ethanol-1-13C_20211029_SuddenSwitch_64Scans.txt');
3     ethZULF = [ethZULF(:,1) abs(ethZULF(:,2))];
4     plot(ethZULF(:,1), ethZULF(:,2));
5
6     spectrum = [x(11:end), ZULF_spectrum_magn(end/2+11:end)];
7

```

end

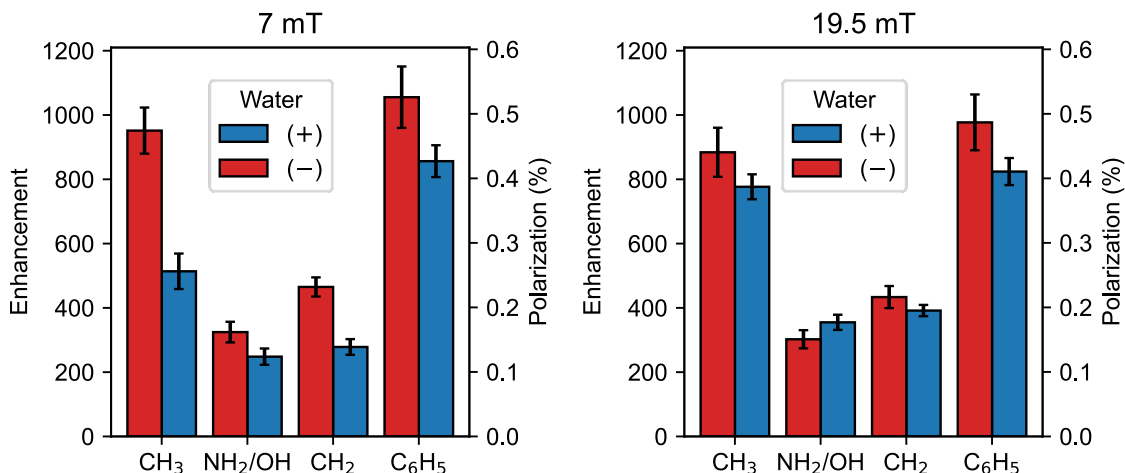


**Figure S4.  $^1\text{H}$  NMR signal enhancements for benzylamine and methanol with and without water added to the sample.** (Sample - 0.5 mL dichloromethane containing 230 mM of methanol, 230 mM of benzylamine, and 12 mM  $[\text{Ir}(\text{IMes})(\text{COD})]\text{Cl}$ ). The sample was bubbled for 10 seconds with  $p\text{H}_2$  at a pressure of 4 bar (gauge) before (red) and after (blue) the addition of 10  $\mu\text{L}$  of water at polarization transfer fields of either 7 mT (left) or 19.5 mT (right). Spectra were taken in a 43 MHz (1 T) SpinSolve benchtop spectrometer (Magritek) and  $^1\text{H}$  NMR signal enhancements were calculated by taking the ratio of SABRE-polarized integrals to the integrals obtained from thermal-equilibrium polarized samples. Sample transfer between polarization transfer field and spectrometer was controlled by robotic arm with an average transfer time of 3 seconds. Error bars represent one standard deviation based on three separate measurements.

0

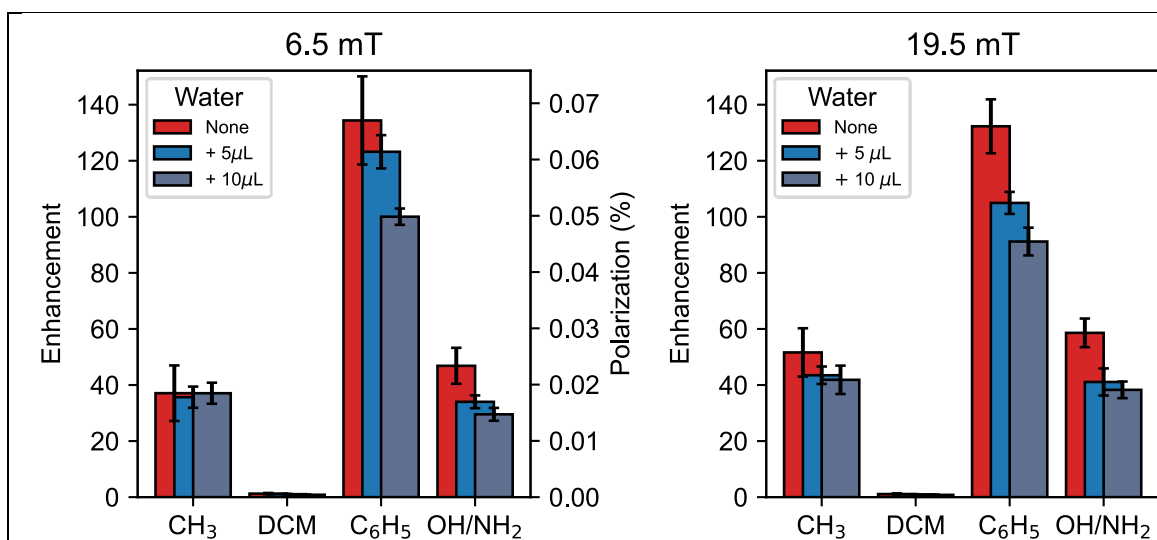


**Figure S5. SABRE-relay  $^1\text{H}$  NMR signal enhancements for ethanol and benzylamine with and without water added to the sample** (Sample - 0.5 mL dichloromethane containing 230 mM of ethanol, 230 mM of benzylamine, and 12 mM  $[\text{Ir}(\text{IMes})(\text{COD})]\text{Cl}$ ). Two times concentrated samples of benzylamine and catalyst were first activated for 10 min under 5 bar of  $p\text{H}_2$  by bubbling at a rate of 20 scc/m. Then a stock solution of ethanol in DCM was added to obtain the final concentrations listed above. Enhancements are calculated as the hyperpolarized integral divided by the thermal equilibrium integral, and polarization is the product of the Boltzmann factor at

1.04 T and the enhancement. Ethanol and benzylamine CH<sub>2</sub> figures are omitted due to significant overlap between the two.

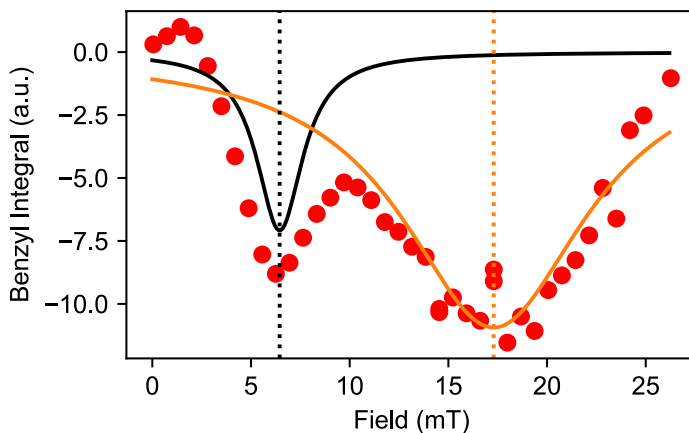


**Figure S6. <sup>1</sup>H NMR integral of SABRE-hyperpolarized benzylamine (-C<sub>6</sub>H<sub>5</sub> group) at varying polarization transfer field. Fitting the data with a double Lorentzian function yields maxima at  $6.5 \pm 0.2$  mT and  $17.3 \pm 0.3$  mT.**

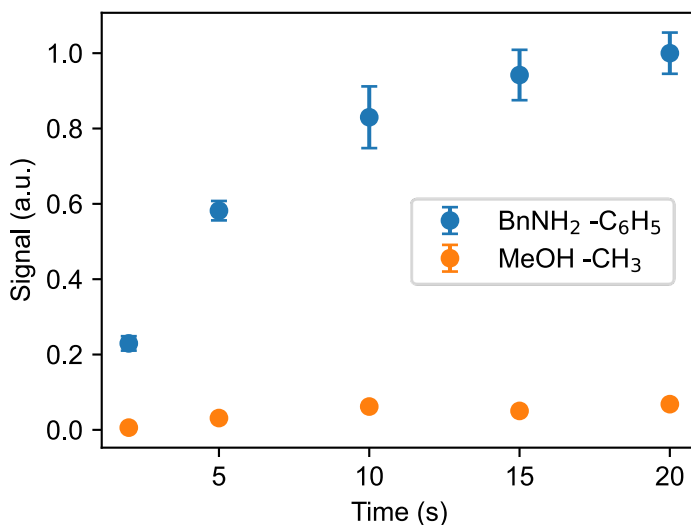


**Figure S7. Polarization buildup curves of benzylamine and methanol.** Solutions containing 230 mM benzylamine (BnNH<sub>2</sub>) and 230 mM methanol (MeOH) with 12 mM [Ir(IMes)(COD)]Cl in dichloromethane were bubbled with *p*H<sub>2</sub> at a rate of 90 scc/m and *p*H<sub>2</sub> pressure of 3 bar (gauge). Error bars are one standard deviation (five separate experiments) and transfer from polarization transfer field to high field for detection was controlled by robotic arm, and spectral acquisition was triggered by Arduino.

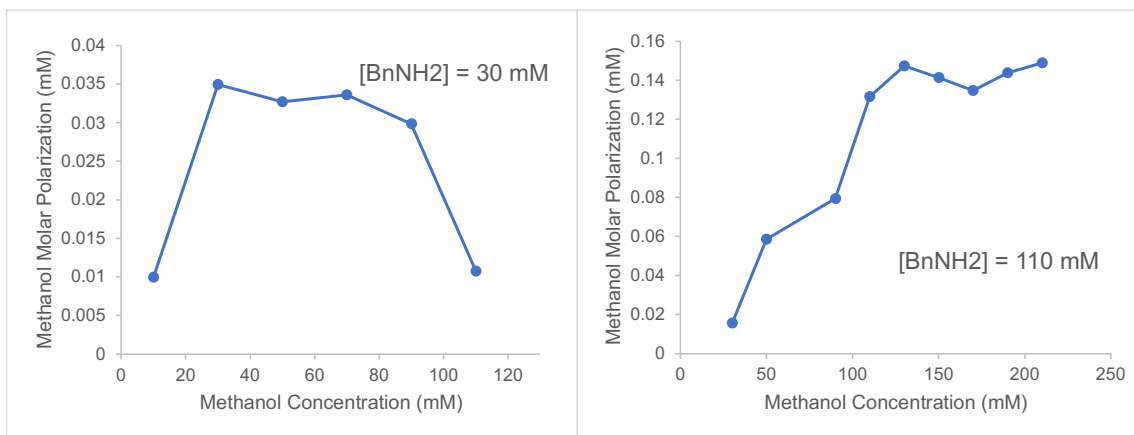


**Figure S8. Optimization of methanol-to-benzylamine ratio.** Molar polarization ( $^1\text{H}$ ) of methanol obtained via SABRE-relay plotted as a function of methanol concentration while the benzylamine ( $\text{BnNH}_2$ ) concentration is kept constant at 30 mM (left) and at 110 mM (right).

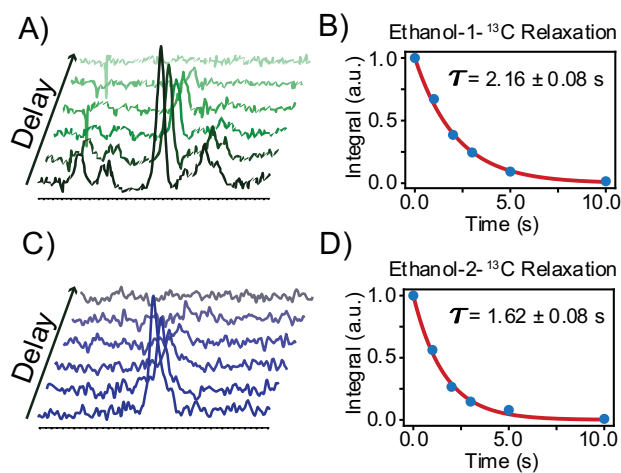
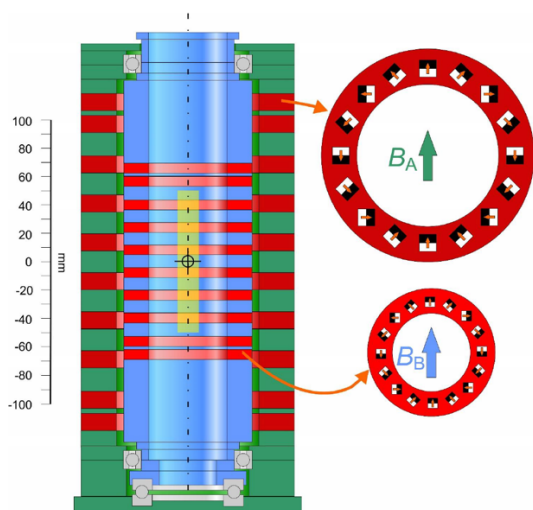


**Figure S9. Relaxometry of ethanol- $1\text{-}^{13}\text{C}$  (A-B) and ethanol- $2\text{-}^{13}\text{C}$  (C-D) at zero field using SABRE-relay hyperpolarization.** Each spectrum is the sum of four scans of a sample containing 230 mM of a labeled ( $1\text{-}^{13}\text{C}$  or  $2\text{-}^{13}\text{C}$ ) ethanol, 230 mM benzylamine and 12 mM  $\text{Ir}(\text{IMes})(\text{COD})\text{Cl}$ . Samples were bubbled in a field of 19.5 mT produced using a solenoid and transferred to zero-field by robotic arm with an average transfer time of 3 seconds.



**Figure S10. Magnet used for upper range polarization transfer field variation experiments.** Magnetic fields used to facilitate transfer of polarization to SABRE substrate above the range of ~25 mT were probed using a variable Hallbach array of magnets designed by Dr. Prof. Peter Blümler.

Sketch of construction:



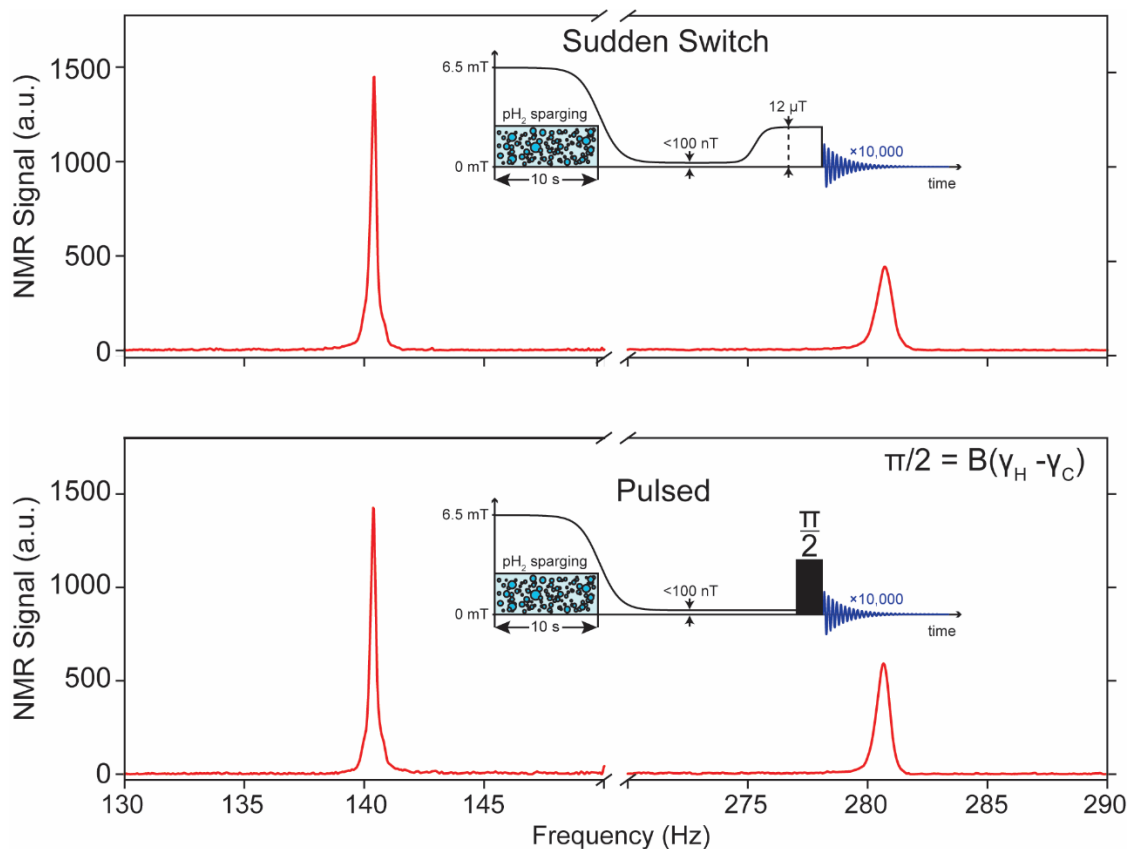


**Figure S11. Comparison between sudden field switch (top) and pulsed (bottom) approaches for recording the ZULF NMR spectra of  $^{13}\text{C}$ -methanol.** Samples were transferred via robotic arm for improved reproducibility between a polarization transfer field of 6.5 mT and detection region inside of an MS-I magnetic shield (TwinLeaf) where fields for manipulation of spins are produced by a Helmholtz array. Pictured schemes represent estimates of the magnetic field experienced by the sample at each point in the transfer process.

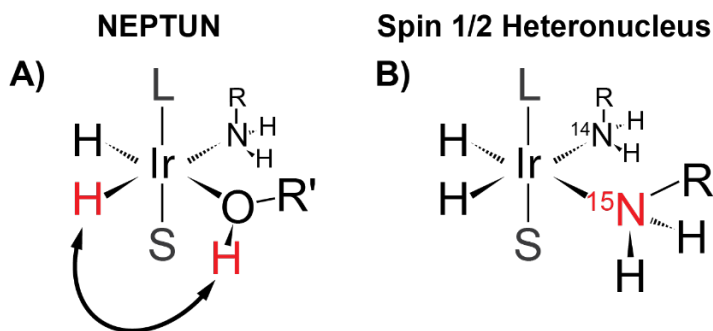


**Figure S12. Two possible complexes contributing to field profile of SABRE efficiency.** In systems using dichloromethane as solvent,  $[\text{Ir}(\text{IMes})(\text{COD})]\text{Cl}$  as the pre-catalyst, benzylamine, and methanol, we have observed increased SABRE efficiency at transfer fields above those expected from currently accepted SABRE-relay theory (39). Two possible mechanisms could be active in addition to the traditional SABRE mechanism modeled by an  $\text{AA}'\text{X}$  three spin system: **A)** NEPTUN (Nuclear Exchange Polarization by Transposing Unattached Nuclei), is based on direct hydride transfer from the catalyst to an axially bound substrate which has a labile proton (46); **B)** Magnetic field dependence complicated by the presence of a heteronucleus, such as  $^{15}\text{N}$ . A single heteronucleus present in the active SABRE complex can split a single maximum in the magnetic field dependence into two (32, 47).

